This is the accepted manuscript made available via CHORUS. The article has been published as:

Effective out-of-plane math xmlns="http://www.w3.org/1998/Math/MathML">mi>g/mi> /math> factor in strained-Ge/SiGe quantum dots

Andrew J. Miller, Will J. Hardy, Dwight R. Luhman, Mitchell Brickson, Andrew Baczewski, Chia-You Liu, Jiun-Yun Li, Michael P. Lilly, and Tzu-Ming Lu

Phys. Rev. B **106**, L121402 — Published 14 September 2022

DOI: 10.1103/PhysRevB.106.L121402

Effective out-of-plane g-factor in strained-Ge/SiGe quantum dots

Andrew J. Miller,* Will J. Hardy, and Dwight R. Luhman
Sandia National Laboratories, Albuquerque, New Mexico 87185 USA

Mitchell Brickson and Andrew Baczewski
Sandia National Laboratories, Albuquerque, New Mexico 87185 USA
Center for Computing Research, Sandia National Laboratories, Albuquerque, New Mexico 87185 USA and
Center for Quantum Information and Control (CQuIC), Department of Physics and Astronomy, University of New Mexico, Albuquerque, New Mexico 87131 USA

Chia-You Liu
Graduate Institute of Electronics Engineering, National Taiwan University, Taipei 10617, Taiwan

Jiun-Yun Li
Graduate Institute of Electronics Engineering, National Taiwan University, Taipei 10617, Taiwan
Taiwan Graduate School of Advanced Technology, National Taiwan University, Taipei 10617, Taiwan and
Taiwan Semiconductor Research Institute, Hsinchu 30078, Taiwan

Michael P. Lilly and Tzu-Ming Lu
Sandia National Laboratories, Albuquerque, New Mexico 87185 USA and
Center for Integrated Nanotechnologies, Sandia National Laboratories, Albuquerque, New Mexico USA

Lithographic quantum dots in strained-Ge/SiGe have rapidly progressed from realization of a single-hole quantum dot to multi-qubit devices. We present a measurement of the out-of-plane g-factor for a single-hole quantum dot in this material. This experiment avoids the strong orbital effects present in the higher p-like orbitals in this configuration and validates the expected g-factor anisotropy. The results are in good agreement with calculations of the g-factor using the heavy- and light-hole spaces of the Luttinger Hamiltonian, showing strong tunability through both the B-field and the charge state.

Semiconductor quantum dots (QDs) are a promising platform for scalable spin-based qubit operations[1–13]. While much research has used silicon-based electron QDs, holes in germanium exhibit many of the same desirable properties, with some beneficial differences: Absence of degenerate valley-states[14], the atomic p-orbital character that naturally suppresses hyperfine induced decoherence[15–18], and large spin-orbit coupling[14, 19] allowing control of qubits using electric dipole spin resonance[15]. Because of these potential advantages, strained-Ge QDs have been under investigation recently[20, 21]. Remarkably, hole-spin qubits in strained-Ge/SiGe heterostructures have progressed quickly from demonstration of a QD to qubit logic[22–25].

The large separation between heavy- and light-hole subbands in this material is enhanced by the strain and confinement within the Ge well. This results in reduced effective off-diagonal terms in a single-band model of the heavy-hole space. The energetic splitting of the $\pm 1/2$ states exceeds the natural spin-3/2 Zeeman term these holes should experience, reducing the mixing of $\pm 3/2$ states by an external magnetic (B)-field. This results in a weak response to B-fields aligned in-plane, indicating a large g-factor anisotropy[26].

This has been confirmed in one-dimensional channels[27] and two-dimensional hole systems where the anisotropy was observed to be density dependent[28]. For single-spin qubits in planar QDs, the magnitude of the anisotropy remains unclear. The in-plane g-factor observed in single-hole qubits is < 0.3[23]. Measurements of the g-factor of a single hole confined to a QD with the B-field directed out-of-plane have not been reported. For multi-hole QDs, $g_\perp$ can be obscured by orbital effects[29], as the alignment of the orbital angular momentum can influence the effective g-factor more than the Zeeman splitting. A highly anisotropic g-factor can be beneficial for qubits. For example, the B-field required for a sufficient Zeeman gap for spin readout would be significantly reduced in the direction with a large g-factor, enabling integration with superconducting elements [25].

We study $g_\perp$ of a QD in strained-Ge/SiGe down to the last hole using magnetospectroscopy. We find an out-of-plane g-factor of 15.7 for a single hole. Using the upper bound of Ref. 23, $g_\parallel = 0.3$, the anisotropy of the g-factor for a single hole confined to a lateral QD is found to be over 50. With increased hole occupancy in the QD ($n > 2$) we observe large changes in the apparent g-factor due to orbital effects. In addition, we perform calculations using the Luttinger Hamiltonian with a realistic QD potential and find remarkable agreement with

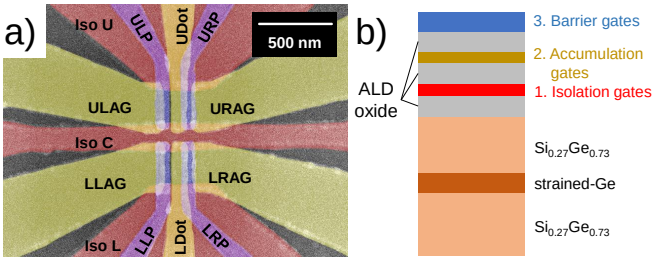


FIG. 1. a) An artificially colorized SEM image of the device design. b) The material stack, using the same color scheme as a). Charge carriers are accumulated in the strained-Ge layer and QDs are formed under UDot and LDot, between the isolation gates.

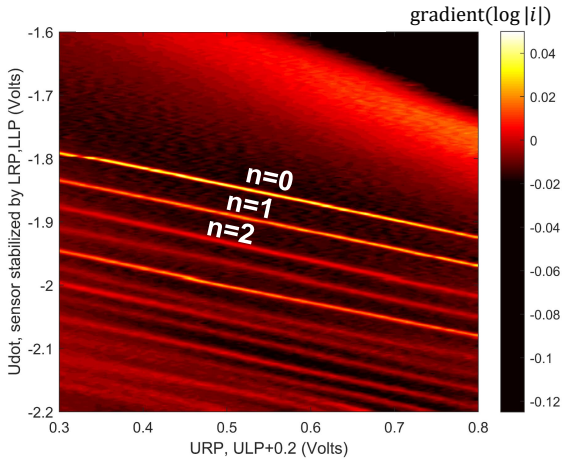


FIG. 2. Stability plot of the QD. The voltage applied to the dot gate is shown on the vertical axis, while the barrier gates (plungers) are displayed horizontally. Color indicates the gradient of the charge sensor current, i. The first three states with n holes present in the dot are labeled.

the single-hole $g_\perp$-factor and also capture the trend for higher occupancy up to six holes.

A strained-Ge quantum well was used as our starting material. The SiGe barriers were 27 % Si, with a 62 nm barrier above the strained-Ge well. The strained-Ge well was 20 nm thick, and showed a mobility of $1.84 \times 10^5\,\mathrm{cm^2\,V^{-1}\,s^{-1}}$ in Hall bar measurements. Growth of the Ge/SiGe heterostructure used the same process described in Ref. 30 with a variation in the SiGe ratio.

Layers of gates were patterned to create a lithographic QD. A scanning electron microscope image of a device can be seen in Fig. 1, along with a schematic of the material stack. By manipulating the voltages of the patterned gate electrodes, charge-carriers (holes) are drawn into the strained-Ge layer, producing a hole gas and hole QDs.

This electrode design defines two single QDs located near each other on the device, labeled as upper and lower, each controlled by five gate electrodes. Prior work developing this design can be found in Ref. 31. Details regarding the device tuning and measurements can be found in the Supplemental Material[32].

The data presented here were taken with an applied out-of-plane B-field in a dilution refrigerator with a base temperature of 30 mK. Magnetospectroscopy measurements were made up to 3 T. The two-dimensional hole gas base temperature was found to be 417(32) mK (see Supplemental Material[32]).

The lower dot was used as a charge sensor, while the upper dot was tuned to the single-hole regime. The coupling between the gate Udot and the QD was measured to be $\alpha = 75.4(35)\,\mathrm{meV\,V^{-1}}$. Fig. 2 shows clearly resolved charge sensing lines.

Magnetospectroscopy was performed with the B-field oriented out-of-plane. Fig. 3 displays typical results. Multiple data sets were taken by sweeping the Udot gate (as in Fig. 3a) and also combinations of ULP and URP with Udot constant. No significant differences were seen in the g-factors obtained by these two types of scans and 10 scans were taken in total.

The data show various kinks as expected for orbital crossings in magnetospectroscopy. Additional near-vertical features around $B = \pm 0.5$ T are also observed. These are likely the result of resonances with quantized states in the two-dimensional reservoir due to the out-of-plane B-field. Our primary concern here is determination of the g-factor near $B = 0$ T, away from these resonances.

Magnetospectroscopy data were analyzed by fitting Gaussians to trace each charge-transition line. The center of each Gaussian fit is highlighted as a red overlay in Fig. 3a. Uncertainty in the position of each Gaussian was determined from the 95 % fit confidence interval. Gate voltage was converted to energy using α and set to zero at $B = 0$ T, as shown in Fig. 3b.

The out-of-plane g-factor, $g_\perp$, is extracted from each scan for the range $B = -0.5$ T to 0.5 T by fitting the difference of the magnetic-field dependent energies, ΔE, from the first two lines to a linear function and relating the slope to the g-factor using $\Delta E = g\mu_B B$, where μ_B is the Bohr magneton. A final value of $g_\perp$ is determined through a weighted average of the results from each scan and the uncertainty in $g_\perp$ is calculated using the standard deviation of $g_\perp$ from the 10 scans. The results of individual scans are displayed in the Supplemental Material[32]. Using this method, we find $g_\perp = 15.7(22)$ for the lowest-lying QD orbital.

Long-term drift was intermittently observed throughout the time that the data were collected and the device required voltage tuning adjustments from scan-to-scan, likely due to trapped charges at the SiGe/oxide interface. Any drift that may have occurred during a single scan is naturally taken into account in ΔE. Small scan-to-scan variation in individual values of $g_\perp$ was random. There

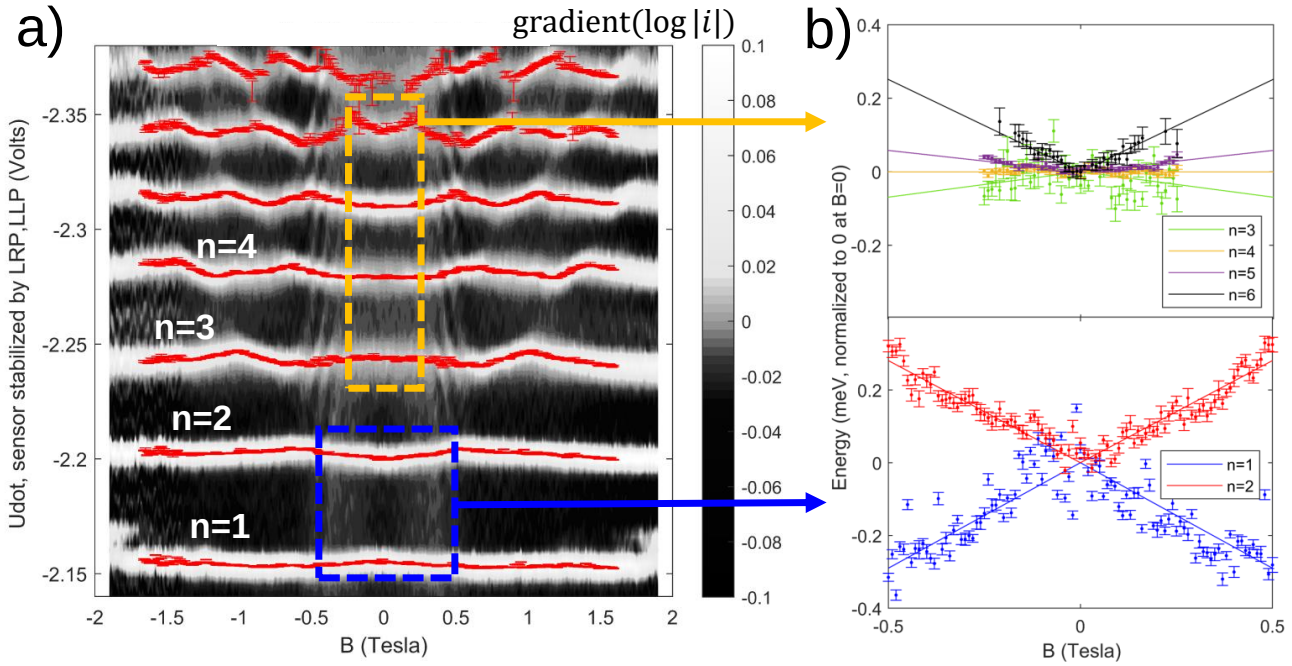


FIG. 3. Magnetospectroscopy of the first several hole transitions. The transition from 0 holes to 1 is labeled $n = 1$ and so on. Ten magnetospectroscopy scans such as a) were taken, although not all scans were able to resolve as many transitions. Seven scans used the Udot voltage to scan across states as shown here, while three scans used the plungers. Greyscale indicates the gradient of the charge sensor current, i. Each line's position was extracted by fitting a Gaussian and is shown by the red overlay. These points were converted to energy, and the region near $B = 0$ was fit using a linear, absolute value function, as shown in b). Each line has been shifted vertically to 0 energy at $B = 0$ to easily compare slopes. The lower plot shows the first two lines, from the s-like orbital, while the upper shows the next four lines, from the p-like orbitals.

was no apparent correlation with tuning or whether Udot or ULP and URP were used to sweep through the dot occupancy levels. This suggests that changes in electric field did not alter the observed value of $g_\perp$ in these experiments. Said differently, any change in $g_\perp$ due to electric field is not resolved within the uncertainty of our experiments.

These out-of-plane measurements yield an experimental result of $g_\perp$ in lithographic, strained-Ge QDs in the single-hole regime. In-plane measurements were made using this same technique on a separate device, shown in Table I, details in the Supplemental Material[32]. The value of the in-plane g-factor in similar devices has been reported as $g_\parallel = 0.2$ to 0.3, depending on device tuning[23]. Taking the upper bound of these more precise measurements on $g_\parallel$, and using our value for $g_\perp$ of 15.7 we find a g-factor anisotropy of $g_\perp/g_\parallel = 52$, much greater than the anisotropy of < 20 reported previously using the Kondo effect[29]. To our knowledge, this is the largest g-factor anisotropy observed among candidate qubits in laterally defined QDs. It is important to note that our measurement of $g_\perp$ was done in the s-orbital of the QD and represents the bare Zeeman g-factor of a hole in a QD with perpendicular applied field.

To further emphasize this, consider a similar analysis using holes in the p-orbital for the range $B = -0.2\,\mathrm{T}$ to $0.2\,\mathrm{T}$. If one were to ignore orbital effects and extract the g-factor from the difference between the $n = 2$ and $n = 3$ states, the effective $g_\perp$ is $-19.0(30)$, and from the difference between $n = 3$ and $n = 4$,$g_\perp = 4.8(40)$, in agreement with recent measurements made using QDs with 3 to 4 hole occupations[25], also included in Table I. This highlights the strong influence of orbital effects on the effective g-factor, and is likely the source of the weaker anisotropy seen in previous transport results obtained with out-of-plane B-fields[29]. With measurements down to the last hole, these results show the expected dramatic anisotropy with respect to the in-plane g-factor, and also indicate a strong variability in the effective g-factor between charge states. This variation in effective g-factor as a function of charge state is also due in part to the strong spin-orbit coupling, an effect which has been seen in other hole-based qubits[22, 26, 33].

To better understand the mechanisms at play, calculations of the QD energy spectrum were performed based on the heavy- and light-hole subbands of the Luttinger Hamiltonian[34].

The QD potential was generated using a COMSOL Multiphysics[35] calculation using the physical device geometry. The potential was then further tuned to the experiment to match the crossing observed between the first and second excited states at $B = 0.6\,\mathrm{T}$ (Fig. 3a)

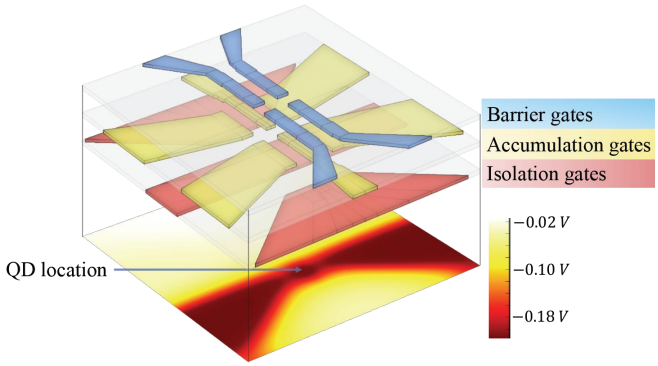


FIG. 4. A wireframe design of the gate layout is included in a COMSOL model of the device. This allows an electrostatic simulation of the accumulation of charge using the Thomas-Fermi approximation for the charge density via a nonlinear Poisson solve. The resulting potential is used as an input to our model of the electronic structure of our hole QD to calculate the eigensates of the potential using an effective mass model.

by adjusting the orbital gap to ≈0.93 meV. This was accomplished by rescaling the potential in the x- and y-dimensions before solving for eigenstates without disturbing the potential in the z-direction.

We numerically study the B-field dependence of the spectrum of single-particle states for a realistic electrostatic model of the device to produce theoretical estimates for the g-factor. Our framework considers the light- and heavy-hole bands simultaneously and solves for the spectrum of eigenstates of the associated Luttinger Hamiltonians including the COMSOL-generated electrostatic potential (Fig. 4)[34, 36, 37]. We do so using an interior penalty discontinuous Galerkin discretization of the associated partial differential equations implemented in an in-house solver. These numerically generated eigenstates are of the full Luttinger Hamiltonian, which explicitly treats the mixing of these bands through spin-orbit coupling. The impact of strain was added in the form of a Bir-Pikus Hamiltonian. This leads to a splitting of the subbands in energy, in which the lower energy single-particle states are dominated by the heavy-hole band. More details can be found in the Supplemental Material[32].

The energy spectrum from the simulation is shown in Fig. 5a. Due to the band gap these states are all spin $\pm 3/2$. The average slope of each line from 0 T to 0.2 T was calculated and is compared with experiment in Fig. 5b. Note that to emphasize the s- and p-orbital nature these are the slopes of individual lines, not the difference in lines used to calculate $g_\perp$ above. The experimental slopes are taken from the data in Fig. 3b.

From these simulations, $g_\perp$ was calculated from the first two levels at 0.2 T using $\Delta E/\mu_B B$ and found to be 16.9, in excellent agreement with the experimental result

TABLE I. Comparison to other measurements

Source	$g_\parallel$	$g_\perp$
Present theory ($Ge/Si_{0.27}Ge_{0.73}$)	0.198	16.9
Present exp. ($Ge/Si_{0.27}Ge_{0.73}$)	—	15.7(22)
Present exp. ($Ge/Si_{0.17}Ge_{0.83}$)	0.23(15)	—
$n > 3$ qubit ($Ge/Si_{0.3}Ge_{0.7}$)[25]	—	4.5 to 6.5
Few-hole qubit ($Ge/Si_{0.2}Ge_{0.8}$)[22]	0.21 to 0.30	—
Kondo Effect ($Ge/Si_{0.3}Ge_{0.7}$)[29]	0.3(1)	5.5(10)
Ballistic holes, 1D channel[27]	0.76 to 1.0	10.4 to 15.0

of 15.7(22). General trends of the experimental data are reproduced by this simulation, including the signs of the slopes and the ordering of their magnitudes. The curvature of each state due to increasing magnetic confinement can also be seen in both experiment and simulation. For the p-orbital states, the simulations correctly reproduce the signs, but overestimate the magnitude. This may suggest that the interactions between holes have a large effect, as those are not accounted for in this single-particle simulation.

Another explanation for the reduced slopes seen in experiment may be due to leakage of the wavefunction into the SiGe barriers, where the g-factor is reduced. The Luttinger parameter is lower in Si than Ge ($|\kappa| \approx 0.42$, compared to ≈ 3.41)[34]. It is expected that $|g| = 6|\kappa|$, and experimentally $g \approx 2$ for holes in Si[38]. This was proposed in Ref. 29 as an explanation for the small $g_\perp$. Due to the agreement in the s-like orbital, it appears that orbital effects and hole-hole interactions are the primary cause of the reduced effective g-factor in higher states, but the g-factor in the SiGe barriers may have some influence.

It is also important to note that although the slopes show repeated signs between lines 3 and 4 as well as 5 and 6, the spin filling follows an alternating pattern, as shown by the color axis in Fig. 5a. These repeated signs are due to the p-like nature of these orbitals. Angular dependence of the phase of the wavefunction in each orbital is aligned with or against classical cyclotron motion, causing the B-field to raise or lower the energy of each state. Stated another way, the orbital angular momentum alignment (anti-alignment) with the B-field causes states 3,4 (5,6) to decrease (increase) with the increasing B-field, overpowering the Zeeman splitting due to the spin state.

Strained-Ge continues to stand out as a promising material for realizing qubits with lithographic QDs. A comparison with previous work can be seen in Table I. This experimental verification of the large g-factor anisotropy in the single-hole regime suggests that a weak B-field can provide a sufficient Zeeman gap in the out-of-plane configuration. Future designs may be able to take advantage of this fact, allowing integration with superconducting elements and the ability to perform spin read-

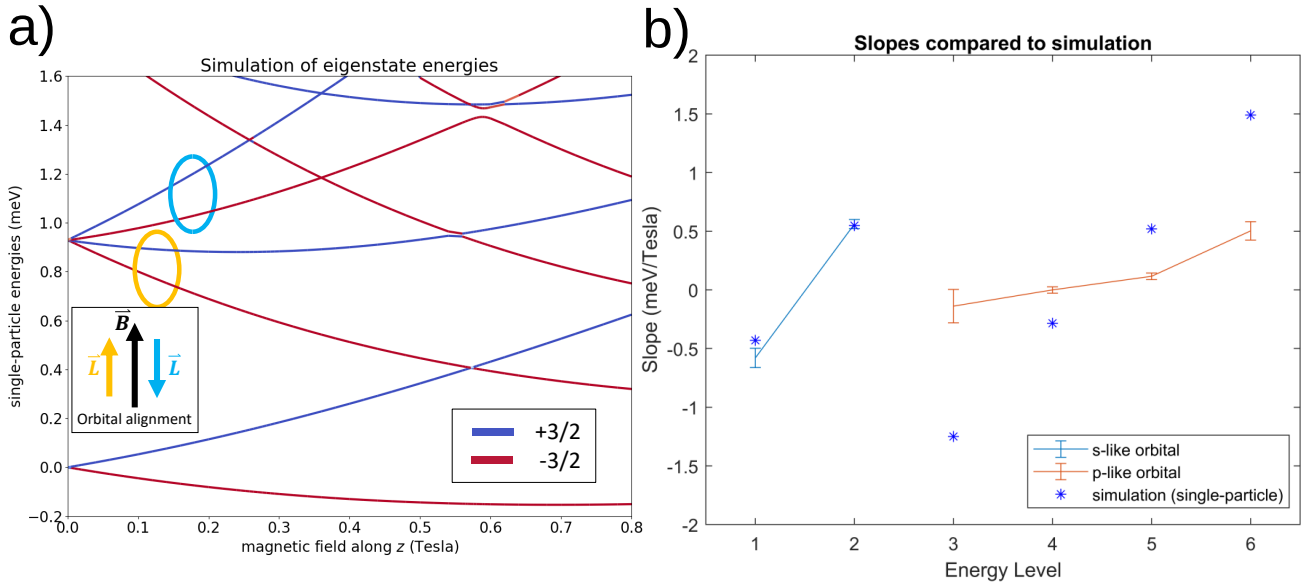


FIG. 5. a) Theoretical calculation of the single-particle energy spectrum for a dot in a potential that is isotropic in the xy-plane. Both the orbital and spin effects on the energy are included. The dominant spin eigenstate is shown by the indicated colors. The splitting between the lowest two states is dominated by the Zeeman splitting, but the upper four states are also impacted by orbital effects. As shown in the inset, the alignment of the orbital angular momentum causes the downward or upward slopes near $B = 0$ in these four lines. b) Comparison between the experimental and theoretical slopes of the energy levels with respect to B-field strength. The simulation shows agreement in the s-like orbital, but only matches the signs of the next 4 p-like states.

out using a B-field produced by on-chip components if desired. These results also highlight the strong orbital-effects present in the out-of-plane case for p-like states. While the simulations presented show good agreement in the single-hole case, they reveal the complexity of the higher-order states. This allows for dramatic tunability of the g-factor via the charge occupation and the B-field, and highlights the difference between g-factor measurements in the single-hole and many-hole regime.

This work was supported by the Laboratory Directed Research and Development Program at Sandia National Laboratories and was performed, in part, at the Center for Integrated Nanotechnologies, a U.S. DOE, Office of Basic Energy Sciences user facility. Sandia National Laboratories is a multimission laboratory managed and operated by National Technology and Engineering Solutions of Sandia, LLC, a wholly owned subsidiary of Honeywell International Inc., for the U.S. Department of Energy's National Nuclear Security Administration under contract DE-NA0003525.

This paper describes objective technical results and analysis. Any subjective views or opinions that might be expressed in the paper do not necessarily represent the views of the U.S. Department of Energy or the United States Government.

The work at National Taiwan University (NTU) has been supported by the Ministry of Science and Technology (110-2622-8-002-014- and 110-2112-M-002-043-) and the Ministry of Education through the Higher Education Sprout Projects (NTU core consortium: 111L892002).

* amille2@sandia.gov

[1] J. R. Petta, A. C. Johnson, J. M. Taylor, E. A. Laird, A. Yacoby, M. D. Lukin, C. M. Marcus, M. P. Hanson, and A. C. Gossard, Science **309**, 2180 (2005).

[2] M. Veldhorst, J. C. C. Hwang, C. H. Yang, A. W. Leenstra, B. de Ronde, J. P. Dehollain, J. T. Muhonen, F. E. Hudson, K. M. Itoh, A. Morello, and A. S. Dzurak, Nature Nanotechnology **9**, 981 (2014).

[3] D. Kim, Z. Shi, C. B. Simmons, D. R. Ward, J. R. Prance, T. S. Koh, J. K. Gamble, D. E. Savage, M. G. Lagally, M. Friesen, S. N. Coppersmith, and M. A. Eriksson, Nature **511**, 70 (2014).

[4] K. Eng, T. D. Ladd, A. Smith, M. G. Borselli, A. A. Kiselev, B. H. Fong, K. S. Holabird, T. M. Hazard, B. Huang, P. W. Deelman, I. Milosavljevic, A. E. Schmitz, R. S. Ross, M. F. Gyure, and A. T. Hunter, Science Advances **1** (2015), 10.1126/sciadv.1500214.

[5] R. Maurand, X. Jehl, D. Kotekar-Patil, A. Corna, H. Bohuslavskyi, R. Laviéville, L. Hutin, S. Barraud, M. Vinet, M. Sanquer, and S. De Franceschi, Nature Communications **7**, 13575 (2016).

[6] P. Harvey-Collard, N. T. Jacobson, M. Rudolph, J. Dominguez, G. A. Ten Eyck, J. R. Wendt, T. Pluym, J. K. Gamble, M. P. Lilly, M. Pioro-Ladrière, and M. S. Carroll, Nature Communications **8**, 1029 (2017).

[7] D. M. Zajac, A. J. Sigillito, M. Russ, F. Borjans, J. M. Taylor, G. Burkard, and J. R. Petta, Science **359**, 439

(2018).
[8] T. F. Watson, S. G. J. Philips, E. Kawakami, D. R. Ward, P. Scarlino, M. Veldhorst, D. E. Savage, M. G. Lagally, M. Friesen, S. N. Coppersmith, M. A. Eriksson, and L. M. K. Vandersypen, Nature **555**, 633 (2018).
[9] W. Huang, C. H. Yang, K. W. Chan, T. Tanttu, B. Hensen, R. C. C. Leon, M. A. Fogarty, J. C. C. Hwang, F. E. Hudson, K. M. Itoh, A. Morello, A. Laucht, and A. S. Dzurak, Nature **569**, 532 (2019).
[10] A. M. J. Zwerver, T. Krähenmann, T. F. Watson, L. Lampert, H. C. George, R. Pillarisetty, S. A. Bojarski, P. Amin, S. V. Amitonov, J. M. Boter, R. Caudillo, D. Corras-Serrano, J. P. Dehollain, G. Droulers, E. M. Henry, R. Kotlyar, M. Lodari, F. Lüthi, D. J. Michalak, B. K. Mueller, S. Neyens, J. Roberts, N. Samkharadze, G. Zheng, O. K. Zietz, G. Scappucci, M. Veldhorst, L. M. K. Vandersypen, and J. S. Clarke, Nature Electronics **5**, 184 (2022).
[11] X. Xue, M. Russ, N. Samkharadze, B. Undseth, A. Sammak, G. Scappucci, and L. M. K. Vandersypen, Nature **601**, 343 (2022).
[12] S. G. J. Philips, M. T. Madzik, S. V. Amitonov, S. L. de Snoo, M. Russ, N. Kalhor, C. Volk, W. I. L. Lawrie, D. Brousse, L. Tryputen, B. P. Wuetz, A. Sammak, M. Veldhorst, G. Scappucci, and L. M. K. Vandersypen, arXiv **2202.09252** (2022), 10.48550/ARXIV.2202.09252.
[13] A. R. Mills, C. R. Guinn, M. J. Gullans, A. J. Sigillito, M. M. Feldman, E. Nielsen, and J. R. Petta, Science Advances **8**, eabn5130 (2022), https://www.science.org/doi/pdf/10.1126/sciadv.abn5130.
[14] R. Moriya, K. Sawano, Y. Hoshi, S. Masubuchi, Y. Shiraki, A. Wild, C. Neumann, G. Abstreiter, D. Bougeard, T. Koga, and T. Machida, Phys. Rev. Lett. **113**, 086601 (2014).
[15] D. V. Bulaev and D. Loss, Phys. Rev. Lett. **98**, 097202 (2007).
[16] C. Testelin, F. Bernardot, B. Eble, and M. Chamarro, Phys. Rev. B **79**, 195440 (2009).
[17] Z. K. Keane, M. C. Godfrey, J. C. H. Chen, S. Fricke, O. Klochan, A. M. Burke, A. P. Micolich, H. E. Beere, D. A. Ritchie, K. V. Trunov, D. Reuter, A. D. Wieck, and A. R. Hamilton, Nano Letters **11**, 3147 (2011), pMID: 21714512, https://doi.org/10.1021/nl201211d.
[18] J. H. Prechtel, A. V. Kuhlmann, J. Houel, A. Ludwig, S. R. Valentin, A. D. Wieck, and R. J. Warburton, Nature Materials **15**, 981 (2016).
[19] C.-T. Chou, N. T. Jacobson, J. E. Moussa, A. D. Baczewski, Y. Chuang, C.-Y. Liu, J.-Y. Li, and T. M. Lu, Nanoscale **10**, 20559 (2018).
[20] W. J. Hardy, C. T. Harris, Y.-H. Su, Y. Chuang, J. Moussa, L. N. Maurer, J.-Y. Li, T.-M. Lu, and D. R. Luhman, Nanotechnology **30**, 215202 (2019).
[21] G. Scappucci, C. Kloeffel, F. A. Zwanenburg, D. Loss, M. Myronov, J.-J. Zhang, S. De Franceschi, G. Katsaros, and M. Veldhorst, Nature Reviews Materials **6**, 926 (2021).
[22] N. W. Hendrickx, D. P. Franke, A. Sammak, G. Scappucci, and M. Veldhorst, Nature **577**, 487 (2020).
[23] N. W. Hendrickx, W. I. L. Lawrie, L. Petit, A. Sammak, G. Scappucci, and M. Veldhorst, Nature Communications **11**, 3478 (2020).
[24] N. W. Hendrickx, W. I. L. Lawrie, M. Russ, F. van Riggelen, S. L. de Snoo, R. N. Schouten, A. Sammak, G. Scappucci, and M. Veldhorst, Nature **591**, 580 (2021).
[25] D. Jirovec, A. Hofmann, A. Ballabio, P. M. Mutter, G. Tavani, M. Botifoll, A. Crippa, J. Kukucka, O. Sagi, F. Martins, J. Saez-Mollejo, I. Prieto, M. Borovkov, J. Arbiol, D. Chrastina, G. Isella, and G. Katsaros, Nature Materials **20**, 1106 (2021).
[26] A. V. Nenashev, A. V. Dvurechenskii, and A. F. Zinovieva, Phys. Rev. B **67**, 205301 (2003).
[27] R. Mizokuchi, R. Maurand, F. Vigneau, M. Myronov, and S. De Franceschi, Nano Letters **18**, 4861 (2018), pMID: 29995419, https://doi.org/10.1021/acs.nanolett.8b01457.
[28] T. M. Lu, C. T. Harris, S.-H. Huang, Y. Chuang, J.-Y. Li, and C. W. Liu, Applied Physics Letters **111**, 102108 (2017), https://doi.org/10.1063/1.4990569.
[29] A. Hofmann, D. Jirovec, M. Borovkov, I. Prieto, A. Ballabio, J. Frigerio, D. Chrastina, G. Isella, and G. Katsaros, arXiv **1910.05841** (2019), 10.48550/ARXIV.1910.05841.
[30] Y.-H. Su, Y. Chuang, C.-Y. Liu, J.-Y. Li, and T.-M. Lu, Phys. Rev. Materials **1**, 044601 (2017).
[31] W. J. Hardy, Y.-H. Su, Y. Chuang, L. N. Maurer, M. Brickson, A. Baczewski, J.-Y. Li, T.-M. Lu, and D. Luhman, ECS Transactions **92**, 17 (2019).
[32] "See supplemental material at [url will be inserted by publisher] for additional details.".
[33] S. D. Liles, R. Li, C. H. Yang, F. E. Hudson, M. Veldhorst, A. S. Dzurak, and A. R. Hamilton, Nature Communications **9**, 3255 (2018).
[34] R. Winkler, *Spin-Orbit Coupling in Two-Dimensional Electron and Hole Systems* (-Verlag Berlin Heidelberg, 2003).
[35] "COMSOL, Inc., COMSOL multiphysics reference manual, version 5.2," (2016).
[36] B. Venitucci, L. Bourdet, D. Pouzada, and Y.-M. Niquet, Phys. Rev. B **98**, 155319 (2018).
[37] B. Venitucci and Y.-M. Niquet, Phys. Rev. B **99**, 115317 (2019).
[38] B. Voisin, R. Maurand, S. Barraud, M. Vinet, X. Jehl, M. Sanquer, J. Renard, and S. De Franceschi, Nano Letters **16**, 88 (2016)